Buried Nonmetallic Object Detection using Bistatic Ground Penetrating Radar with Variable Antenna Elevation Angle and Height

Yu Zhang¹, Dan Orfeo¹, Dylan Burns¹, Jonathan Miller², Dryver Huston¹, Tian Xia¹

¹School of Engineering, University of Vermont, Burlington, VT, USA

²White River Technologies, Inc., Lebanon, NH, USA

ABSTRACT

Ground penetrating radar (GPR) has been shown to be an effective device for detecting buried objects that have little or no metal content, such as plastic, ceramic, and concrete pipes. In this paper, buried non-metallic object detection is evaluated for different antenna elevation angles and heights using a bistatic air-launched GPR. Due to the large standoff distance between antennas and the ground surface, the air-launched GPR has larger spreading loss than the hand-held GPR and vehicle-mounted GPR. Moreover, nonmetallic objects may have similar dielectric property to the buried medium, which results in further difficulty for accurate detection using air-launched GPR. To study such effects, both GPR simulations and GPR laboratory experiments are performed with various setups where antennas are placed at different heights and angles. In the experiments, the test surface areas are configured with and without rocks in order to examine surface clutter effect. The experimental results evaluate the feasibility and effectiveness of bistatic air-launched GPR for detecting buried nonmetallic objects, which provide valuable insights for subsurface scanning with unmanned aerial vehicle (UAV) mounted GPR.

Keywords: Ground penetrating radar (GPR), bistatic radar, dielectric constant, buried object detection, non-destructive evaluation

1. INTRODUCTION

There is a high demand for non-contact subsurface imaging for the detection and identification of buried objects. Of particular interest is the detection of buried objects with little to no metal content. Ground penetrating radar (GPR) has been proved to be an effective system for detecting such objects, such as plastic, ceramic, and concrete pipes [1]-[6]. Based on antenna configurations, GPR can be classified as ground-coupled GPR or air-launched GPR. Ground-coupled GPR has antennas installed at close proximity to the detection surface, which results in high detection sensitivity and small signal loss. However, the near contact required of ground-coupled GPR presents hazards to equipment and personnel when searching for buried objects. For certain application, i.e. mine detection, ground-coupled GPR are not deployable [7]. For air-launched GPR, the antennas are typically operated at heights greater than one-quarter of the operating wavelength. Compared to ground-coupled GPR, the use of an air-launched GPR sensing provides the benefit of contactless survey on a large area in a short period of time [8], which will reduce the risk of entering inaccessible or hazardous areas for GPR operators.

A bistatic radar is comprised of a transmit antenna and a receive antenna which are separated by a close distance in comparison with the distance from either antenna to the subsurface target [9]. In buried object detection, the GPR signal undergoes various losses in its propagation path from the transmitter to the receiver. Due to the large standoff distance between antennas and the ground surface, air-launched GPR signal has a large loss. Moreover, a target of low metal content may have similar dielectric property to the buried medium, necessitating a high degree of sensitivity [10]. Any equipment configuration represents an effort to diminish each of these obstacles, while recognizing that certain tradeoffs are necessary.

In this study, various realistic antennas setups for air-launched GPR are tested. Tests also included the consideration of objects of different dielectric properties, shapes, sizes and different sand-surface conditions. The experimental results explore the feasibility and effectiveness of air-launched GPR for the detection of buried nonmetallic objects, which are of values for mounting GPR on an UAV to leverage inspection performance.

2. EXPERIMENTAL METHODS

2.1 Testbed

A 1.8-meter-wide by 1.8-meter-long sandbox testbed was built to facilitate buried-target GPR testing. The testbed is constructed almost entirely of wood, to avoid using metal material that might cause interference to GPR operations and signal fidelity. Sand is filled to a depth of 19 cm. Figure 1(a) shows the 3D SolidWorks CAD model for the sandbox test bed; Figure 1(b) shows the testbed frame built according to the CAD design. With this testbed, antenna height, angle, and separation can be adjusted. Data is collected as antennas are manually moved across the sandbox to perform the scan.





(b)

Figure 1 Sandbox testbed

2.2 Equipment and targets

In the test, a Keysight N9917A FieldFox Handheld Microwave Analyzer (30 kHz -18 GHz) is used for radar signal transmission and reflection signal acquisition. A pair of ultra-wide bandwidth horn antennas [11] are employed whose operating frequency ranges from 500 MHz to 6 GHz. For performance evaluation, a commercial ground-coupled 2.3 GHz GPR system, MALÅ Concrete Explorer (CX) is adopted as the reference system. In Table 1, the objects for each test case and their corresponding dimension parameters are listed.

Plastic			Metal Wire			Air Gap
White Round	<u>Grey</u> <u>Round</u>	Uneven Surface	<u>Coaxial</u>	<u>10 AWG</u>	Belden 9332	Nonmetallic with wires
Diameter: 26 cm	Diameter: 20.5 cm	Diameter: 11 cm	Diameter: 1 cm		Multi-conductor 9 pairs 22 AWG	Length: 52 cm
Height: 8 cm	Height: 5.8 cm	Height: 3.8 cm		•		Width: 6.4 cm Height: 3.8 cm

Table 1: Targets used in GPR testing

2.3 Diagram of antenna angles setup

Since the horn antenna is directional antenna, the angle offset between the target and the antenna's main beam has a significant impact on the GPR image's quality [11]. Experiments on various antenna elevation angles are performed to examine such effects. The test setup diagram is shown in Figure 2(a). The angle of each antenna is measured up, from vertical, as shown in Figure 2(b). For each pair of transceiver antennas, the angles of transmitter and receiver antennas are measured as θ_1 and θ_2 respectively. The *antenna angle*, Θ , is the sum the angles of the two antennas, i.e. $\theta = \theta_1 + \theta_2$. For example, if the transmit antenna has an angle of 45° and the receive antenna has an angle of 45°, then $\Theta = 90^{\circ}$.

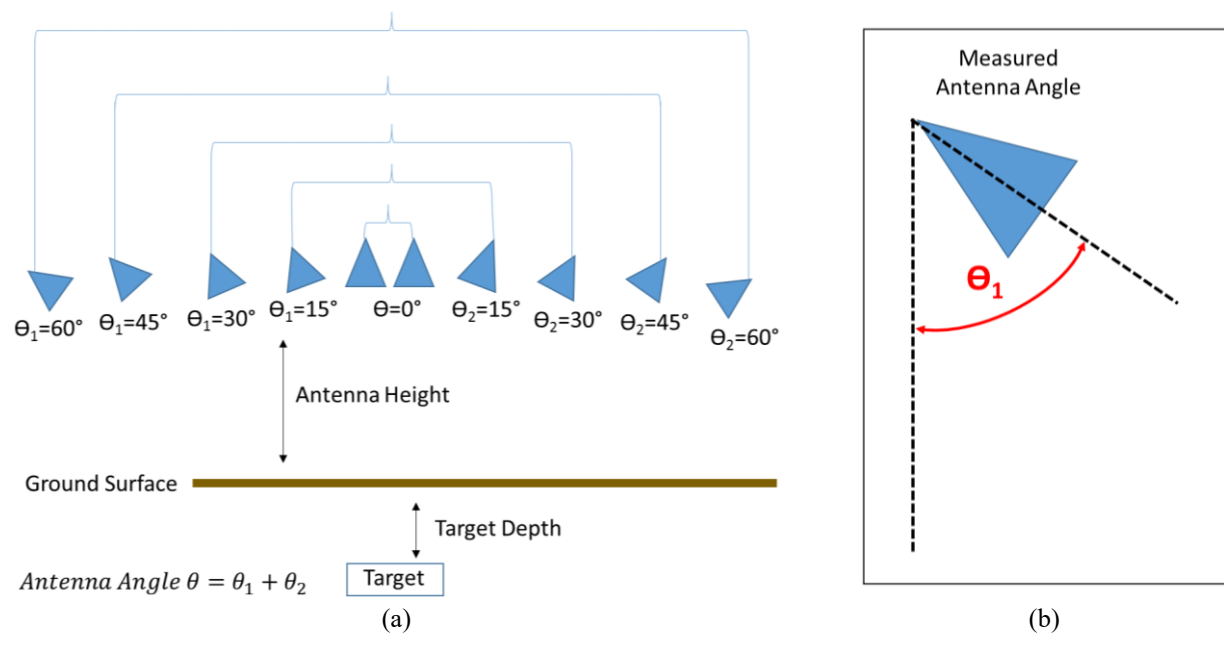
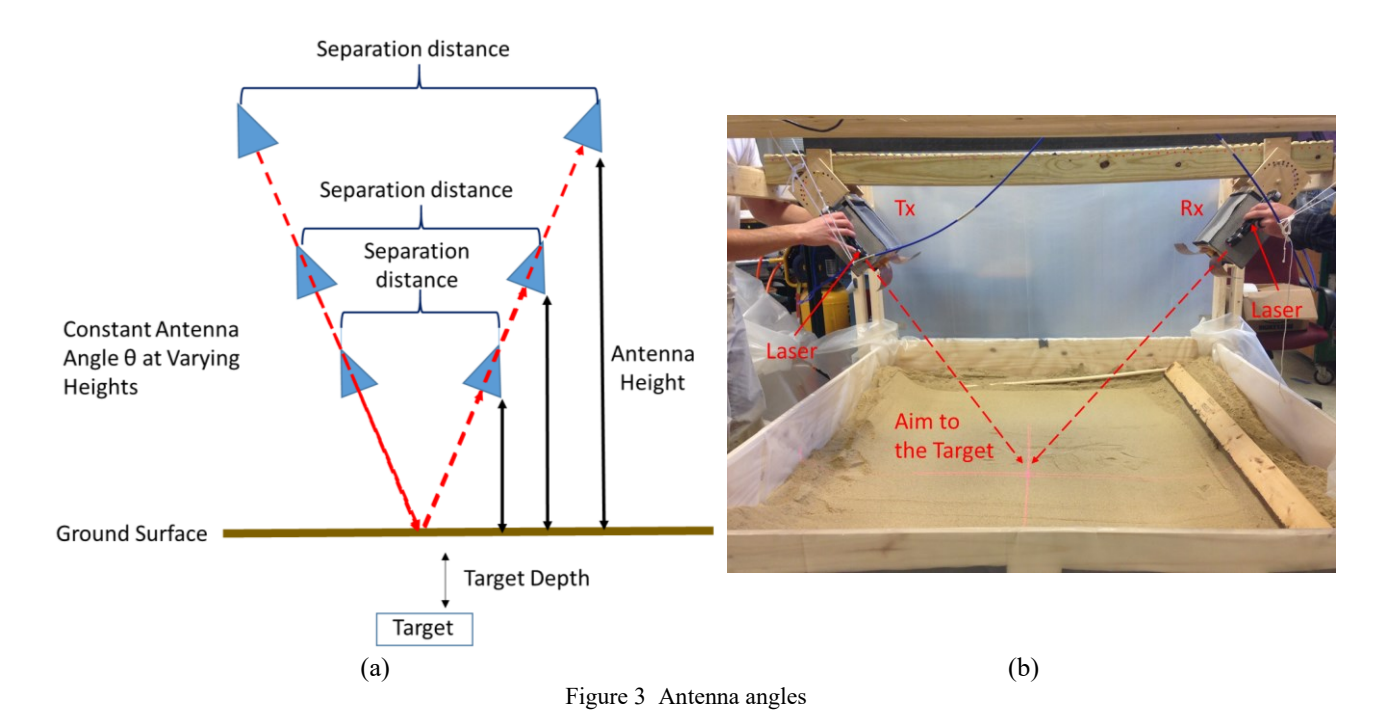


Figure 2 Antenna angles

2.4 Diagram of antenna heights setup

For air-coupled GPR system, a higher standoff distance between the antennas and ground ensures the flexibility of system movement, however, the higher standoff distance also results in large signal loss during the transmission. Such tradeoff should be taken into consideration when the antenna height is tuned [12]. Experiments on various antenna height are conducted to investigate the impact of antennas height on the GPR sensing. The experiment diagram is shown in Figure 3(a), in which for a fixed antenna elevation angle, different antenna standoff heights are evaluated. Since the horn antenna is directional, a calibration step is first performed to ensure the antenna's main beam is aiming at the target. As shown in Figure 3(b), two laser pointers are utilized to align the main beams of transceiver antennas to a focus point.



3. ANTENNA HEIGHT EXAMINATION EXPERIMENTS

In this part of study, tests were performed to examine performance when GPR antennas were placed at different heights, i.e. 48 cm, 61 cm, 71 cm, 91 cm, and 119 cm. To evaluate the measurement results, the test was first conducted using GPRMAX simulation program [13]. As shown in Figure 4, a grey plastic object was used as the target in the tests, whose diameter is 20.5 cm and thickness is 8.5 cm. The dielectric constant values of different media are presented in Table 2.

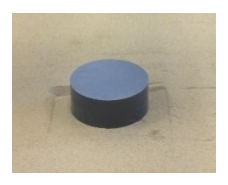


Figure 4 Grey plastic round as the target under test

Table 2 Dielectric constants used in GPRMAX simulation

	Air	Sand	Grey Target
Dielectric Constant	1	3.12	3.27

3.1 Height examination using GPRMAX simulation software

In each GPRMAX height simulation, 121 A-scans were produced. The amplitude of the direct coupling between the antennas, as well as the amplitude of the signal reflected from the sand surface, were measured. The results are shown Figure 5(a).

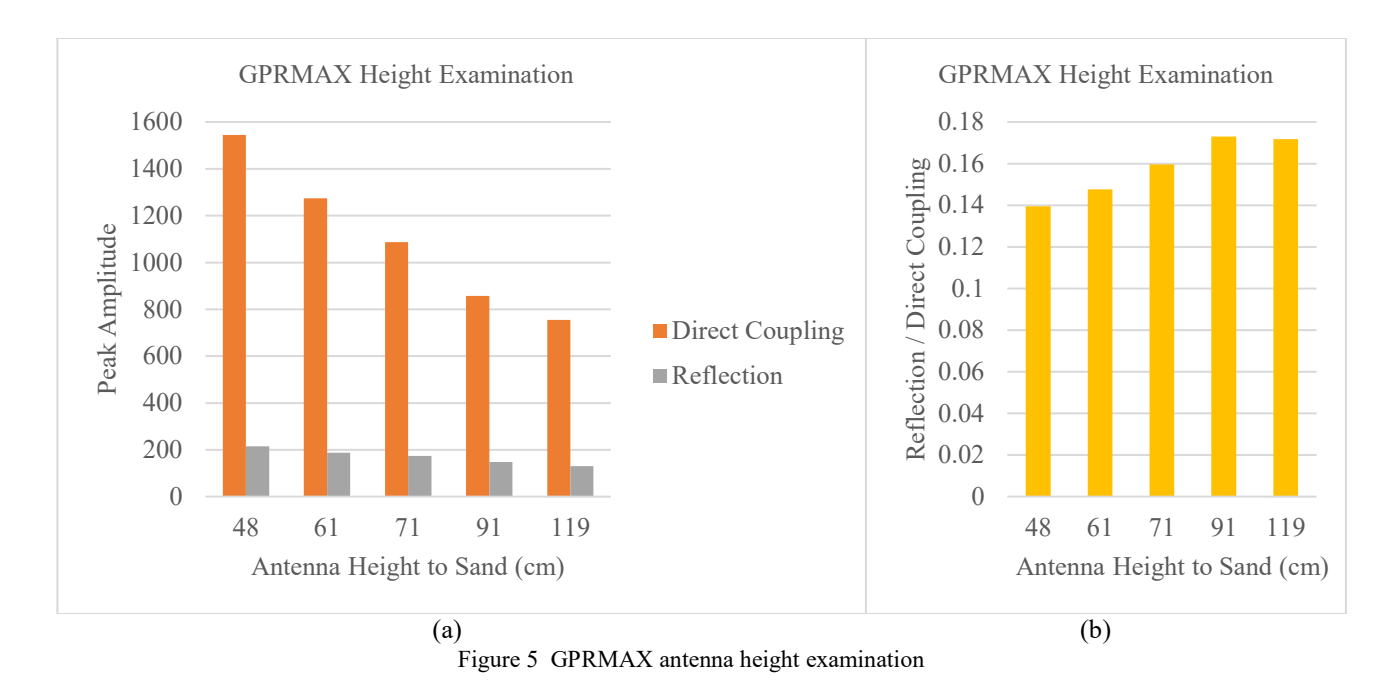


Figure 5(b) shows the ratio of $\frac{Reflection\ Amplitude}{Direct\ Coupling\ Amplitude}$ for each antenna height. The greater this ratio, the better the GPR performance. Performance increases up to the 91 cm height, and then levels-off, decreasing slightly, which indicates that the optimal height is around 91 cm.

3.2 Laboratory height examination

Antenna separation distance for each height was set to 64 cm, 74 cm, 89 cm, 99 cm, 145 cm respectively. The grey plastic target was buried at a depth of approximately 8 cm, and the sand surface was raked flat. To minimize edge effects caused by the testbed for all the heights tested, both the transmit and receive antennas were set to an angle of 30° , for a total $\Theta = 60^{\circ}$. For the test of each height, 38 A-scans were taken. The distance interval between two scans is 1 inch. For each A-scan, the average values of the antenna direct coupling signals, as well as the sand surface reflection signals, were characterized, and are plotted in Figure 6(a).

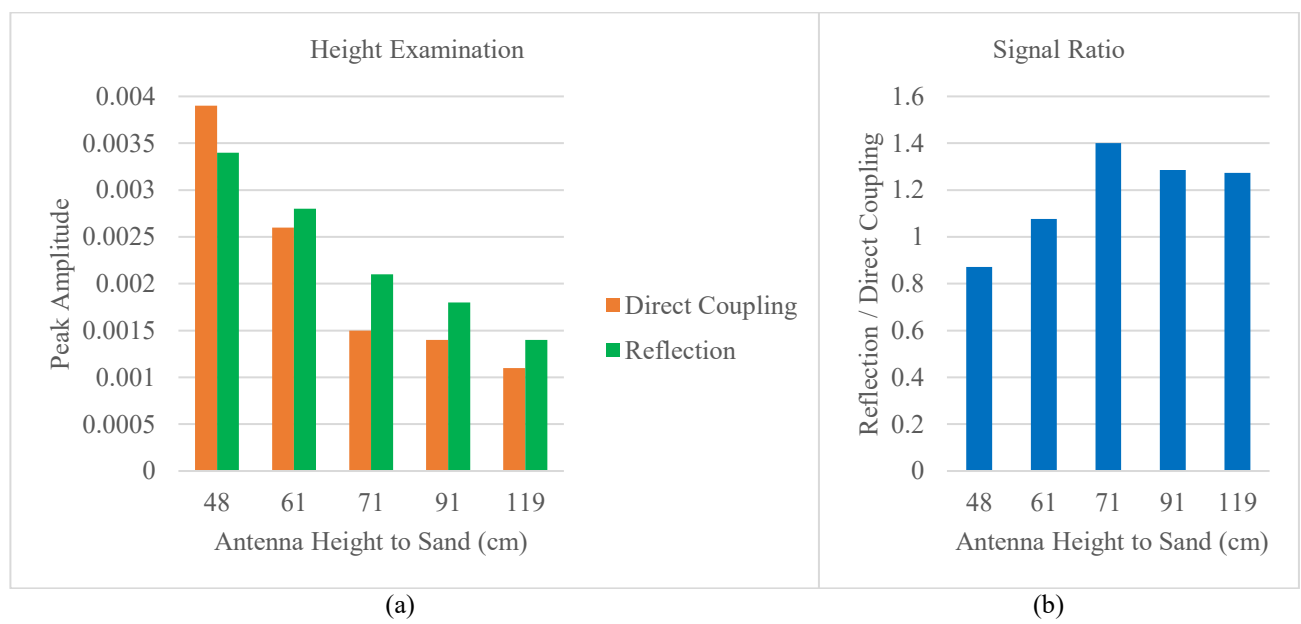


Figure 6 Antenna height examination

Figure 6(b) shows the ratio of $\frac{Reflection\ Amplitude}{Direct\ Coupling\ Amplitude}$ for each antenna height. As can be observed, the value of the ratio increases up to the 71 cm height, and then decreases only slightly, which indicate that the maximum ratio is likely achievable in between 71 cm and 91 cm. Such a result is approximately consistent with the GPRMAX simulations.

4. ANTENNA ANGLE EXAMINATION

Antenna angle is another variable that should be investigated for GPR performance. Different test cases were performed to examine antenna angle effect. In each test case, the angles of transmit and receive antennas are identical. Five angle combinations were tested: transmit and receive antennas both set at 0° , 15° , 30° , 45° , and 60° , correspondingly, the antenna angle is $\theta = 0^{\circ}$, 30° , 60° , 90° , and 120° . The grey plastic target was chosen for consistency with height optimization testing.

4.1 Signal strength

The optimized antenna standoff height of 71 cm was adopted. At each angle, 38 A-scans were taken, one inch apart, as the antennas were moved together across the sandbox. For each A-scan, the amplitude of the direct coupling between the antennas, as well as the reflected signal amplitude from the sand surface, were measured, shown in Figure 7(a).

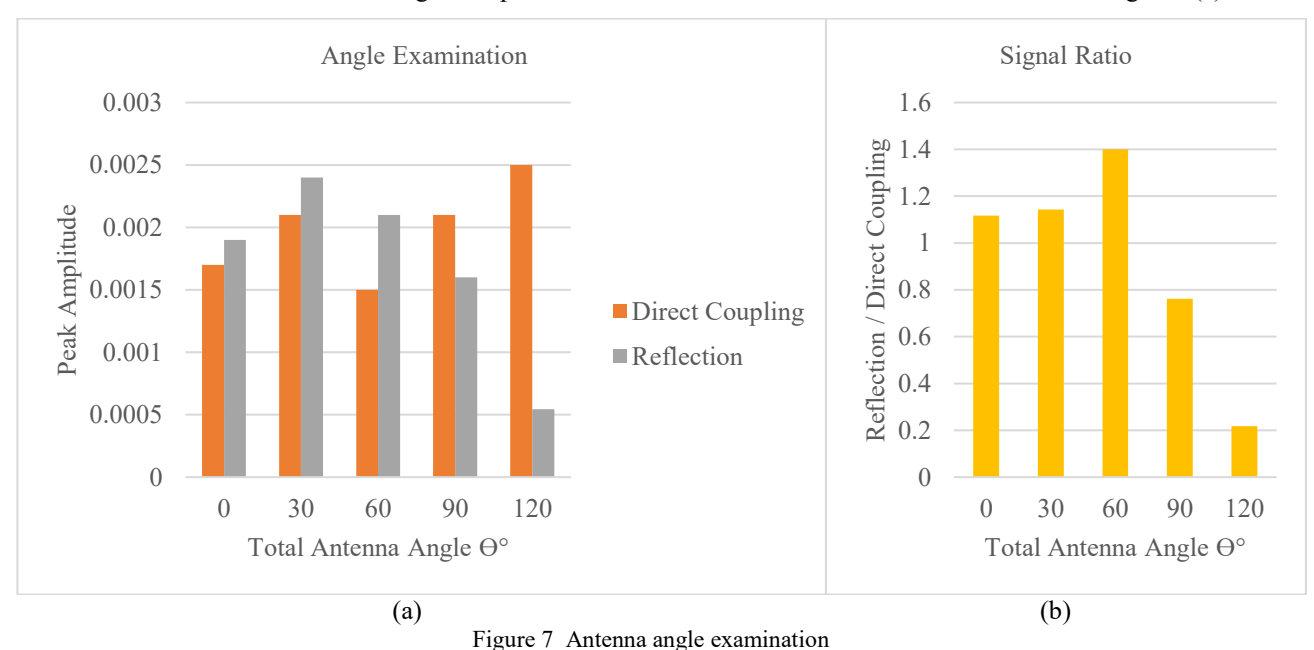


Figure 7(b) shows the ratio of $\frac{Reflection\ Amplitude}{Direct\ Coupling\ Amplitude}$ for each antenna angle. From this metric, it can be concluded that a combined antenna angle of $\Theta=60^{\circ}$ produces the best results for nonmetallic object detection in the sandbox testbed. Future tests can be designed with consideration for this preferred configuration.

5. LABORATORY GPR TESTS

For this series of laboratory tests, antenna height was configured such that the vertical distance between the antennas and the sand surface was 71 cm. In the test, each target was covered with approximately 8 cm of sand. Antennas were configured to be compatible with the requirements of a forward-looking GPR system [13]. As illustrated in Figure 8, in a forward-looking GPR system, the transmit antenna is mounted in front of a vehicle, and has a large standoff distance to inspect the underground target area. The receive antenna is mounted on an UAV. The forward-looking GPR system is capable of collecting data for a much larger area in a much shorter time [14]. This requires that the angle of the transmit antenna should be large in order to achieve a wide inspection area coverage. On the other hand, the angle of transmit antenna should be around 30° to achieve a high radar detection capability. To balance these design goals, the transmit antenna and receive antenna are both set to 45°, for a total value of $\Theta = 90^{\circ}$. Measurements were taken every inch as the antennas were moved horizontally over the buried target in the sandbox testbed.

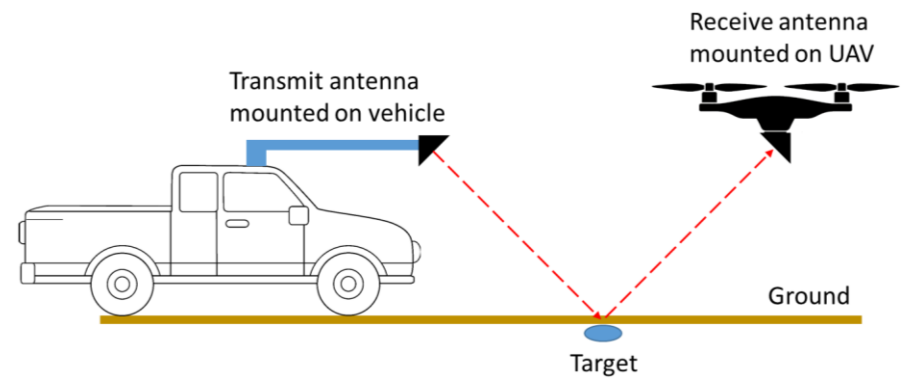


Figure 8 Forward-looking GPR system

5.1 Surface variation with black plastic round

The round black plastic target was buried in the sandbox testbed for GPR experiments. Real-world GPR surveying includes uneven terrain and surface clutter. System performance is evaluated for both clutter and non-clutter test scenarios. The test with no surface alterations was performed first. The B-scan image is plotted in Figure 9.

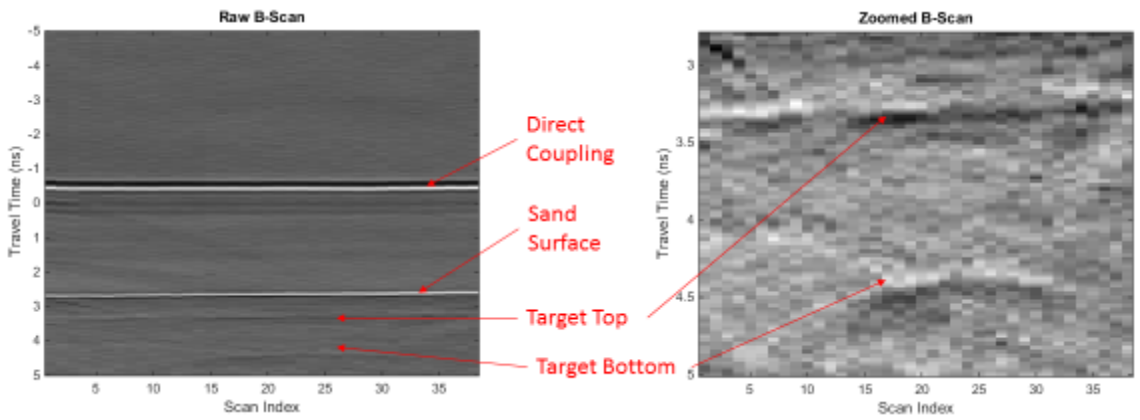


Figure 9 B-Scan image for round black plastic target

The two different surface variation configurations are shown in Figure 10. In Figure 10(a), rocks and bricks were arranged on the sand surface to provide surface clutter. These were removed in Figure 10(b), and a series of approximately 7 cm tall, parallel sand-ridges were sculpted.



Figure 10 Surface clutter (a) and surface variation (b)

B-Scan images from the surface clutter tests are shown in Figure 11. The target's hyperbola pattern is clearly visible, as in the case of the previous test without surface alterations.

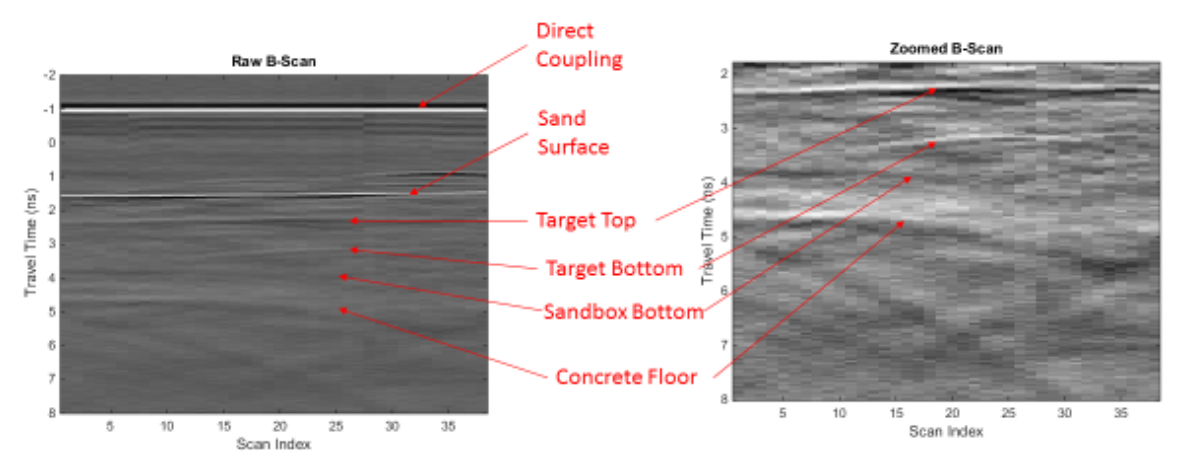


Figure 11 B-Scan image for black plastic round target with surface clutter

The B-scan image for the surface variation test is shown in Figure 12. The signal is not appreciably deteriorated by the uneven sand surface.

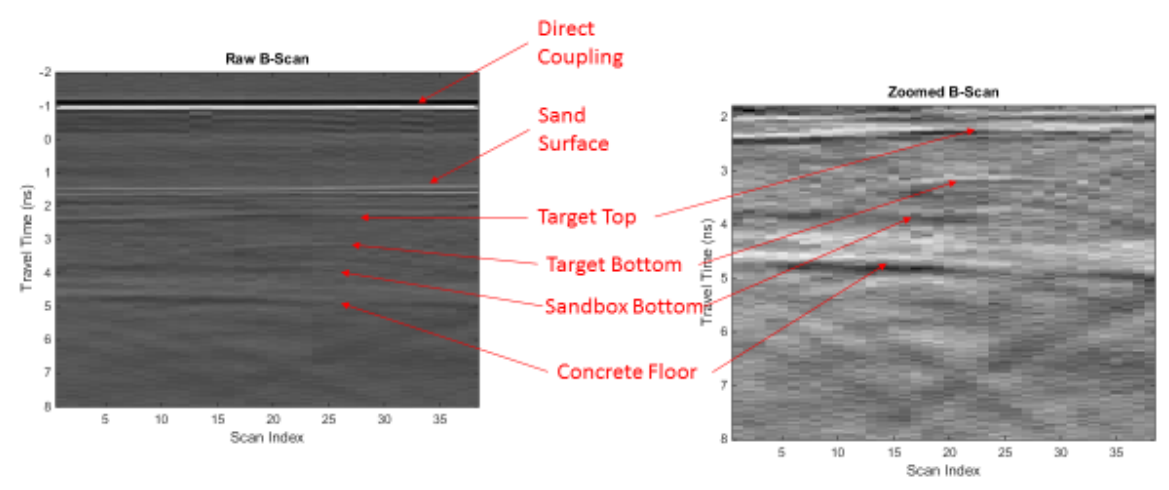


Figure 12 B-Scan image for round black plastic target with surface variation

5.2 Buried wire

Metal wires are often present in, or near, subterranean man-made devices. Detection of these wires may lead to easier positive identification of this class of buried object [15]. Three metal wires were buried parallel to one another: a shielded braided coaxial with 1 cm outer diameter, an insulated Belden 9332 multi-conductor with 9 pairs of 22 AWG, and a 10 AWG insulated wire. The test setup is shown in Figure 13, in order from left to right. Data were collected in 1 inch increments as the antennas were manually moved forward over the buried wires in the sandbox testbed, perpendicular to the direction of the buried wires.



Figure 13 Antenna movement perpendicular to buried wires

After the data collection, the data were read into the data processing program, and B-Scan images were created, as shown in Figure 14. Notice that three distinct hyperbolas are visible, and that these hyperbolas are comparably well-defined, in spite of the differences in wire thickness.

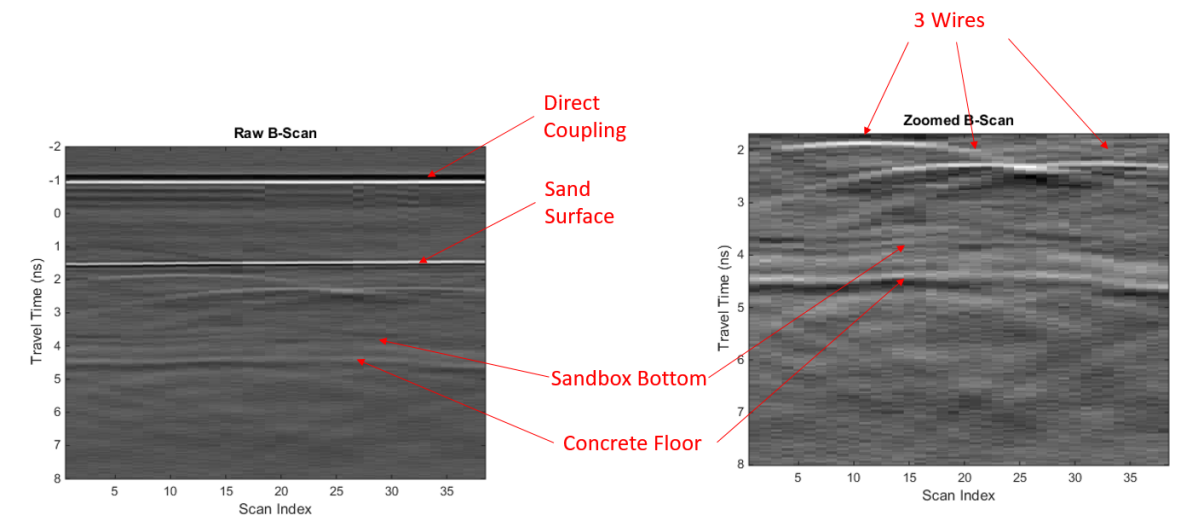


Figure 14 B-Scan image for buried wire test using the air-coupled GPR system

For validation, the ground couple GPR system MALÅ Concrete Explorer (CX) was also used to collect data over the same buried wires. Results are shown in Figure 15. The ground-coupled MALA GPR produces steeper hyperbolas due to the greater angular resolution afforded by being ground-coupled and closer to the target.

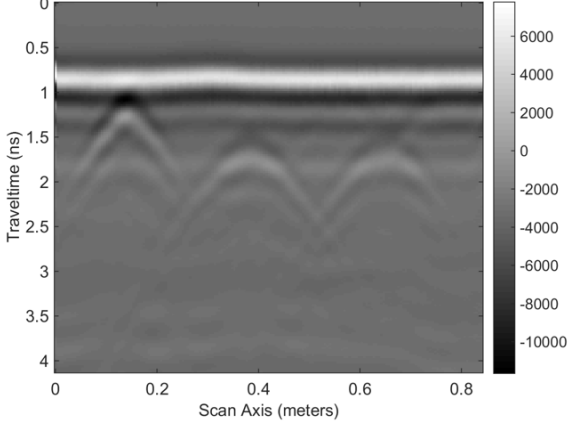


Figure 15: B-Scan image for buried wire test setup in sand box using the commercial ground-coupled Mala GPR system

5.3 Buried air gap with connected wires

Air gap detection provides a way to find the empty spaces that are often present in buried man-made devices ^[16]. As shown in Figure 16, a wooden non-metallic box with an air gap and connected wires was buried in the testbed. The air-coupled GPR system was used to perform scan in 1 inch increments as the antennas were manually moved forward over the buried target in the sandbox testbed.



Figure 16 Buried object with air gap and attached wires in sandbox

The raw B-scan image, shown as Figure 17(a), does not yield clear features. Figure 17(b) enlarges the area-of-interest, revealing muddled hyperbolas. While features are present, it is difficult to distinguish the air gap from the wires without prior knowledge of their relative positions, much less to distinguish the wires from each other. Despite this, the air-launched GPR is able to detect the presence of the air gap target.

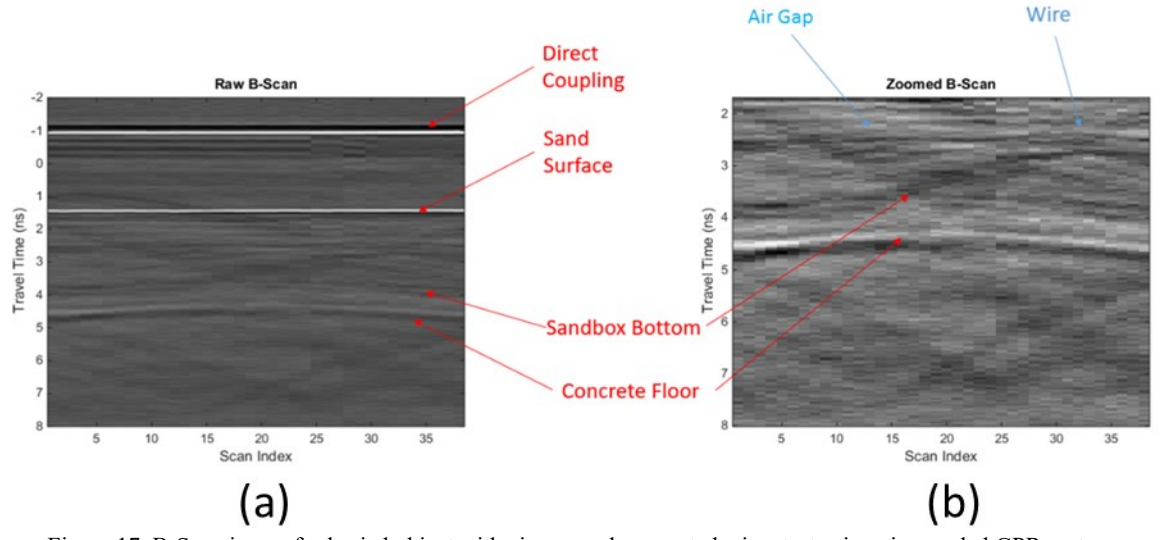


Figure 17 B-Scan image for buried object with air gap and connected wires test using air-coupled GPR system

The ground coupled MALÅ GPR was also used in the test for result verification. Results from the MALÅ scan are shown in Figure 18. As expected, the ground-coupled system is able to resolve the features more clearly than the air-launched GPR.

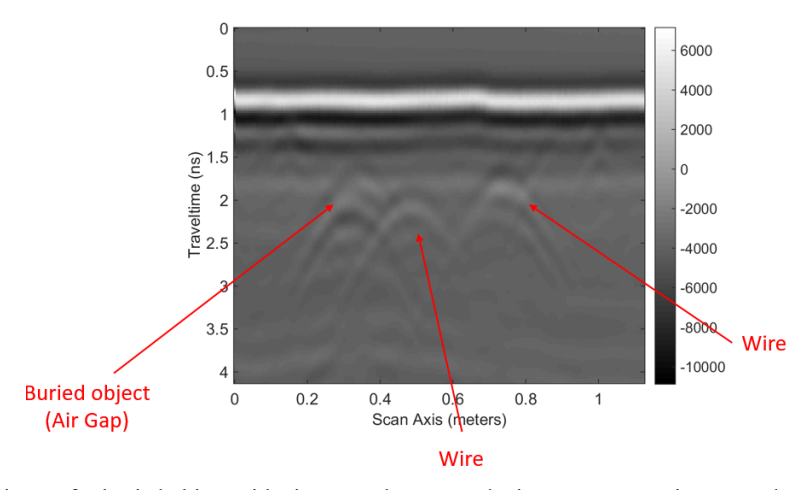


Figure 18 B-Scan image for buried object with air gap and connected wires test setup using ground-coupled MALA GPR

5.4 Buried object with non-uniform top surface

Many artificial devices have non-uniform top surfaces. A round, nonmetallic target with a non-uniform top surface was buried in the sandbox testbed as shown in Figure 19.



Figure 19 Buried object with non-uniform top surface in sandbox testbed

The B-scan image is shown in Figure 20. A feature present in the raw B-Scan image is clearly distinguishable as a target in the zoomed-in right panel. Notice also the diagonal lines visible in the zoomed portion, which are indicative of edge-effects caused by dimensional constraints of the sandbox testbed. The surface irregularities of the target do not appear to significantly deteriorate air-launched GPR performance.

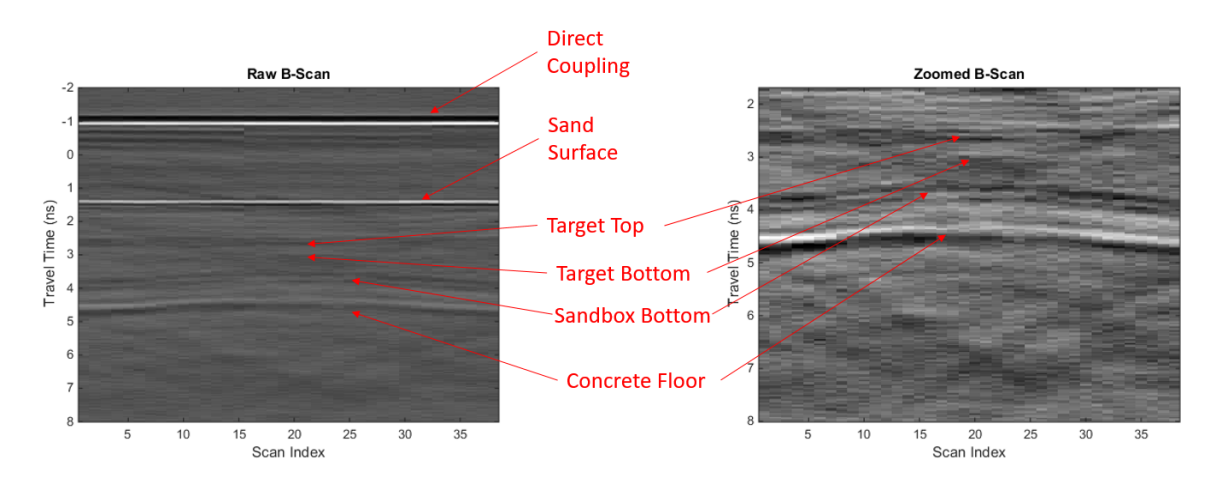


Figure 20 B-Scan image for buried object with non-uniform top surface using air-coupled GPR system

As shown in Figure 21, data taken with the ground-coupled MALA GPR again produces a steeper hyperbola from which it is easier to determine the exact location of the target. The overall strength of the feature, however, appears comparable to that produced with the air-launched GPR.

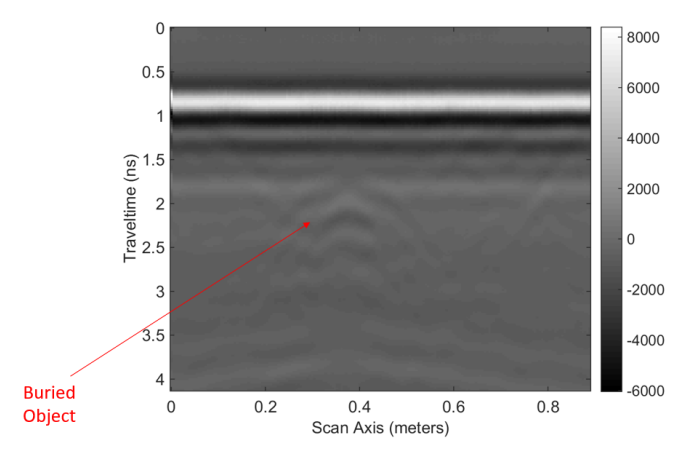


Figure 21 B-Scan image for buried object with non-uniform top surface test using Mala GPR system

6. DISCUSSIONS AND CONCLUSIONS

In this paper, antenna configurations of various heights and elevation angles have been examined. In next step, more comprehensive studies will be conducted to different combinations of antennas elevation angle and height. Currently, due to the physical size limitations of the sandbox testbed, the tunable resolution of both height and elevation angle are rough, and the tunable range is limited. More sophisticated studies will also be performed in future work.

For some GPR subsurface inspection scenarios, the transceiver antennas might operate at approximately near field region. Due to the complexity of the antenna radiation pattern at near field region, hence more investigations of the near field performance of air-coupled GPR need to be conducted in both analytic and experimental ways.

Forward-looking GPR system design requirements were considered in our examinations. However, due to the size limitation of the sandbox testbed and indoor lab space, such examination is still at its early stage. In future work, more outdoor experiments will be performed to evaluate antennas setups for forward-looking GPR system mounted on terrestrial vehicle and/or UAV.

In summary, laboratory tests and computer simulations have been conducted to explore the feasibility of air-launched GPR for the detection of buried nonmetallic objects. A process was developed to optimized antenna height, and antenna angle. Such study is of value for the design of air-launched GPR systems, specifically for those mounted on UAV.

Evaluation of the current air-launched system with a commercially available ground-coupled GPR system reveals situations in which the air-launched system performs comparably. Further optimizations is necessary to improve the performance of the air-launched GPR for detecting certain classes of object.

ACKNOWLEDGEMENTS

This research was support in part by U.S. National Science Foundation grants 1647095 and 1640687, and U.S. Army contract/grant W911NF-13-1-0301.

REFERENCES

- [1] Jol, H. M., [Ground Penetrating Radar Theory and Applications], Elsevier (2008).
- [2] Venkatachalam, A.S., Xu, X., Huston, D., and Xia, T., "Development of a New High Speed Dual-Channel Impulse Ground Penetrating Radar," IEEE Journal of Selected Topics in Applied Earth Observations and Remote Sensing 7(3), 753-760 (2014).
- [3] Huston, D., Hu, J. Q., Maser, K., Weedon, W., and Adam, C., "GIMA ground penetrating radar system for monitoring concrete bridget decks," Journal of Applied Geophysics 43, 139-146 (2000).
- [4] Zhang, Y., Venkatachalam, A.S., Huston, D. and Xia, T., "Advanced signal processing method for ground penetrating radar feature detection and enhancement," Proc. SPIE 9063, 906318 (2014).
- [5] Zhang, Y., Candra, P., Wang, G., and Xia, T., "2-D entropy and short-time Fourier transform to leverage GPR data analysis efficiency," IEEE Transactions on Instrumentation and Measurement 64(1), 103-111 (2015).
- [6] Zhang, Y., Venkatachalam, A.S., Xia, T., Xie, Y., and Wang, G., "Data analysis technique to leverage ground penetrating radar ballast inspection performance," In Proceedings of 2014 IEEE Radar Conference (2014).
- [7] Daniels, D. J. [Ground penetrating radar, vol. 1], IET (2004).
- [8] Xia, T, Venkatachalam, A., Zhang, Y., Burns, D., and Huston, D., "Performance Enhanced High Speed UWB GPR System for Buried Rebar Detection," Symposium on the Application of Geophysics to Engineering and Environmental Problems, (2013)
- [9] Willis, N. J., [Bistatic radar, vol. 2], SciTech Publishing (2005).
- [10] Sai, B., Morrow, I., and Genderen, P. V., "Limits of detection of buried landmines based on local echo contrasts," In Proc. 28th EuMc Workshop, 121-125 (1998).
- [11] Ahmed, A., Zhang, Y., Burns, D., Huston, D., and Xia, T., "Design of UWB Antenna for Air-Coupled Impulse Ground-Penetrating Radar," IEEE Geoscience and Remote Sensing Letters 13(1), 92-96 (2015).
- [12] Kang, W., Kim, C. R., Kim, J. H., Park, S. G., Cho, S. J., Son, J. S., and Kim, K. W., "A study of antenna configuration for bistatic ground-penetrating radar," In 2016 16th International Conference on Ground Penetrating Radar (GPR), 1-4 (2016).
- [13] Giannopoulos, A., "Modelling ground penetrating radar by GPRMAX," Construction and Building Materials 19(10), 755-762 (2005).
- [14] Wang, Y., Li, X, Sun, Y., Li, J., and Stoica, P., "Adaptive imaging for forward-looking ground penetrating radar," IEEE Transactions on Aerospace and Electronic Systems 41(3), 922-936 (2005).
- [15] Chen, C. C., Higgins, M. B., O'Neill, K., and Detsch, R., "Ultrawide-bandwidth fully-polarimetric ground penetrating radar classification of subsurface unexploded ordnance," IEEE Transactions on Geoscience and Remote Sensing 39(6), 1221-1230 (2001).
- [16] Daniels, D. J., "Ground penetrating radar for buried landmine and IED detection," In Unexploded Ordnance Detection and Mitigation, Springer Netherlands, 89-111 (2009).